

## Extracting aquaculture ponds from natural water surfaces around inland lakes on medium resolution multispectral images



Zhe Zeng<sup>a</sup>, Di Wang<sup>a,d</sup>, Wenxia Tan<sup>b,\*</sup>, Jianhua Huang<sup>c</sup>

<sup>a</sup> School of Geosciences, China University of Petroleum, Qingdao 266580, China

<sup>b</sup> Key Laboratory for Geographical Process Analysis & Simulation of Hubei Province/College of Urban and Environmental Sciences, Central China Normal University, Wuhan 430079, China

<sup>c</sup> National & Local Joint Engineering Research Center of Satellite Navigation and Location Service, Guilin University of Electronic Technology, Guilin, 541004, China

<sup>d</sup> Wuhan University, Wuhan 430079, China

### ARTICLE INFO

#### Keywords:

Aquaculture pond  
Inland lake  
Shape feature  
Landsat  
Gaofen-1

### ABSTRACT

A considerable portion of the natural inland lakes has been gradually transformed into aquaculture ponds to meet the enormous demand for aquaculture products. The changes in ponds area can be used to measure the impact of human activities on inland lakes. However, aquaculture ponds and inland lakes are often intermingled with each other especially in the areas close to the lake shore, posing great difficulties for the extraction of aquaculture ponds from medium resolution (15–30 m) multispectral imagery, such as Landsat TM, OLI, and Geofen-1 WFV images. This study proposes a contour-based regularity measurement for water segments, which evaluates the zero-curvature portions of the boundaries, to distinguish aquaculture ponds from natural water. Water surfaces are firstly extracted from satellite images, and then boundary trace of each water segment is carried out to evaluate the geometrical feature of its contour, including perimeter, curvature and the proposed contour-based regularity. Eventually, SVM classification based on these geometrical features separates the aquaculture ponds from inland lakes. Experiments on Landsat TM, OLI, and Geofen-1 WFV images showed that the combination of perimeter, area and proposed contour-based regularity outperforms other feature combinations and produced the most accurate classification. Therefore, the proposed method can be used to extract all aquaculture ponds from all historic Landsat images to monitor the changes in inland aquaculture.

### 1. Introduction

Inland lakes around urban areas are greatly affected by human activities due to intense development in China. Due to high demand of aquaculture products for urban population of neighboring metropolis (Ottinger et al., 2016; Froehlich et al., 2017), many inland lakes that are close to large cities are gradually turned into aquaculture ponds. Aquaculture ponds are shallow artificial water bodies with distinctly man-made shape for aquaculture production (Tran et al., 2015). Most of these aquaculture ponds are always full of water, but some are partially or fully dry in the harvest season (Ottinger et al., 2017). These ponds around inland lakes are formed gradually by embankment, including the partition and regularization of lake water bodies. Similar to coastal aquaculture (Bengil and Bizzel, 2014; Gusmawati et al., 2018), the development of fish pond farming in inland lakes have been causing large-scale land-use changes around lakes, including the destruction of wetlands and the pollution of lakes and soil.

Remote sensing is an effective means for globally monitoring of lake surface water extent (Verpoorter et al., 2014; Tebbs et al., 2015; Palmer et al., 2015; Sheng et al., 2016; Pekel et al., 2016; Urbanski et al., 2016; Shi et al., 2017; Wu et al., 2017), including monitoring the process of gradually transforming lake water bodies into aquaculture ponds. Water index- and threshold- based approaches are extensively performed for large scale water bodies mapping from multi-spectral remote sensing satellite imagery by incorporating various spectral characteristics of water in different bands (Zhou et al., 2017). The commonly used water extraction indices are NDWI (Normalized Difference Water Index, McFeeters, 1996), MNDWI (Modified Normalized Difference Water Index, Xu, 2006), NDMI (Normalized Difference Moisture Index, Rokni et al., 2014), WRI (Water Ratio Index, Rokni et al., 2014), AWEI (Automated Water Extraction Index, Feyisa et al., 2014), etc.

Classification methods are often used to discriminate and extract aquaculture ponds from natural water surfaces. Using SPOT5 and Worldview-1, a semi-automatic classification procedure that employed

\* Corresponding author.

E-mail address: [tanwenxia@mail.ccnu.edu.cn](mailto:tanwenxia@mail.ccnu.edu.cn) (W. Tan).

unsupervised clustering for aquaculture pond extraction with the aid of visual inspection was proposed (Gonario and Virdis, 2014). Through the combination use of a Landsat image and a SPOT5 image, the maximum likelihood classification was used to get the long-term land use change in a delta area of Vietnam, in which aquaculture pond was one of the classes (Tran et al., 2015).

In the remote sensing community, the geometric shape presentation is extensively used for identifying objects in satellite images. Geometrically presenting an object in the image is mainly characterized by shape descriptors (Zhang and Lu, 2004; Kurnianggoro et al., 2018). A crown shape model is presented for Scots pine and Norway spruce recognition in optical remote sensing (Rautiainen et al., 2008). Alpha shape is introduced for identifying curvature of overpass mountain roads in IKONOS images (Alian et al., 2014). Both crown shape model and alpha shape are descriptors that geometrically approximate objects. However, identifying the artificial structures in complex context needs the feature descriptor which can geometrically measure the man-made shape. For example, shape features, including area, length-width ratio, compactness and structure local binary pattern descriptor, are integrated for detecting ships in 2 m spatial resolution images from Google Earth (Yang et al., 2017). Shape compactness and shape index are used to extract the aquaculture ponds in coastal area by image segmentation of Sentinel-1 Synthetic Aperture Radar (SAR) (Ottinger et al., 2017). However, the shape metric used for SAR is not necessarily suitable for medium resolution multi-spectral satellite imagery. Furthermore, identifying artificial objects similar to fish ponds on satellite images also requires profiling the shape regularity. Fourier transform is employed to evaluate the repetition part of boundary, which indicates shape regularity, to distinguish artificial regions in high-resolution satellite images (Eskandari et al., 2012). However, the boundaries are not necessarily repetitive features for fish ponds. Parallel or vertical segment structures in region boundaries are described as the shape regularity for identifying raft cultivation in high-resolution images (Wang et al., 2017), which is essentially a structural region-based descriptor. The boundaries of aquaculture ponds may not only include parallel or vertical segments, but also oblique lines and curves. The most distinguished feature of aquaculture ponds compared to nearby inland

lakes on medium resolution satellite images is that ponds always have some straightness parts in the boundary. Therefore, the discrimination of fish pond and nearby inland lakes requires regularity features that can globally measure the extent of straightness.

Previous studies for aquaculture ponds extraction normally use satellite images that have spatial resolutions equal to or higher than 10 m (Gusmawati et al., 2018). For instance, fish ponds in coastal region were identified from the 10 m Sentinel-1 SAR images (Ottinger et al., 2017). Nevertheless, monitoring aquaculture ponds around inland lakes on a long-term scale requires satellite images that have been recorded for several decades. These images, such as Landsat images, usually have much lower spatial resolution. Although an algorithm for aquaculture ponds extraction in coastal areas from the Landsat TM images was proposed (Zhang et al., 2010), it is not suitable for inland aquaculture ponds. Firstly, inland lakes and ponds are generally smaller in size. Secondly, inland lakes are often surrounded by several other land cover types that make the scene much more complex. Moreover, quite many aquaculture ponds close to inland lakes have been transformed from the shore area of natural lakes, and sometimes aquaculture ponds and lake surfaces are similar in size. Due to the complicated context of fish ponds and inland lakes, separating aquaculture ponds from inland lakes using multi-spectral satellite images is a challenge, not to mention the study of long-term changes of aquaculture ponds.

To overcome the difficulties in separating aquaculture ponds from surrounding inland lakes, geometric differences between natural lakes and aquaculture ponds will be examined in this study. As the water surfaces of natural lakes wind along the local terrain, their boundaries are generally extremely irregular. Thus, the boundaries of natural water surfaces are more curved or meandering because the natural water flow follows the topography and conforms to the curvature of the Earth's surface. On the other hand, the outlines of aquaculture ponds are constructed in straight lines to delimit the boundary in a local area for saving construction costs. Thus, the boundaries of aquaculture ponds have a more regular shape globally compared to those of the natural water surfaces. The aims of this study are to (1) develop geometrical features that are capable of characterizing the difference between natural lakes and aquaculture ponds; (2) use the proposed features to

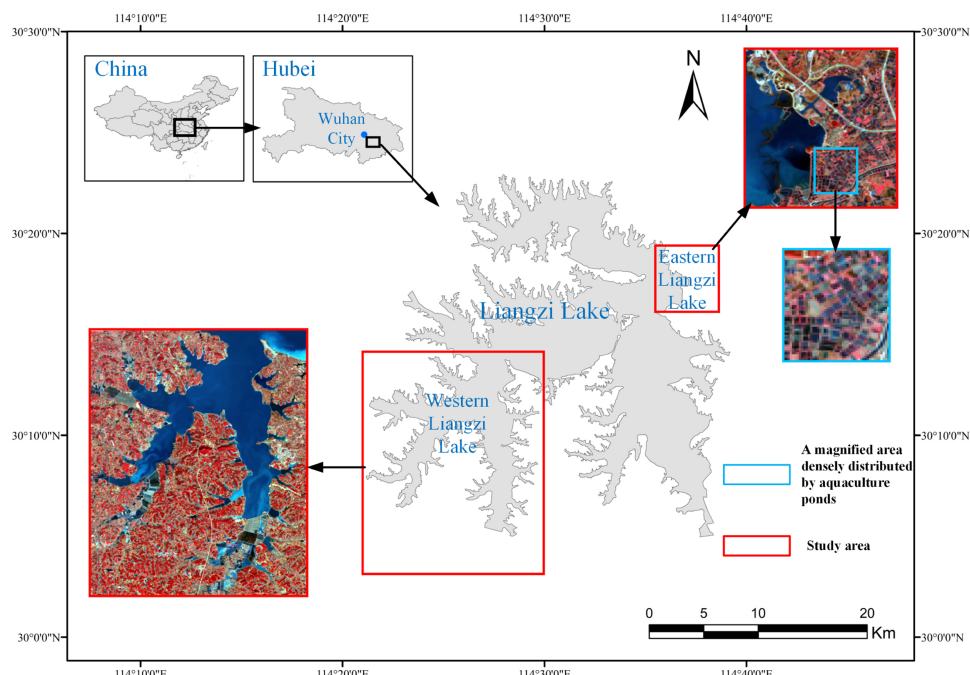


**Fig. 1.** Location of Liangzi Lake in Hubei Province and the two experimental regions in the eastern and western part of the Lake. The satellite images used are acquired by Landsat OLI with pseudo color synthesized by Band 5, 4 and 3.

extract aquaculture ponds from multi-spectral satellite images with spatial resolution of 16–30 m (coarser than 10 m); and (3) evaluate the performance of the aquaculture pond extraction method.

## 2. Study area and data

Hubei is an inland province in central China densely distributed with thousands of lakes. The lakes in Hubei have undergone tremendous changes with the loss of natural lakes and the gradual increase of aquaculture ponds since the late 1970s due to four decades of rapid economic development. Liangzi Lake, located in the southeastern Hubei and neighboring to Metropolis Wuhan, is one of the largest lakes in Jianghan Plain of Hubei ( $30^{\circ}4'–30^{\circ}20'N$  and  $114^{\circ}21'–114^{\circ}42'E$ , Fig. 1). Liangzi Lake has a total area of approximately  $225\text{ km}^2$  in the annual average water level (Qin et al., 2016). Quite many neighboring areas of Liangzi Lake have been partly transformed into aquaculture ponds due to human disturbance.

Two representative branches of Liangzi Lake were selected as study areas, as shown in Fig. 1. The eastern Liangzi Lake study region is an area with densely distributed aquaculture ponds. The western lake study region has a mixture of natural lake water surfaces with aquaculture ponds that were transformed from the neighboring area of natural lake surfaces.

Images from two satellites are employed to test the proposed method: Landsat launched since July 23, 1972 with the potential for monitoring the long-term changes of inland lakes (Wulder et al., 2012, 2016), and Gaofen-1, which is a high-resolution Chinese Earth observation Satellite launched on April 26, 2013, with the capability of providing near real-time (temporal resolution of 4 days or less) imagery of Earth (Sun et al., 2018). In this study, Landsat images from Thematic Mapper (TM) and Operational Land Imager (OLI) with a spatial resolution of 30 m and Gaofen-1 images from Wide Field of View (WFV) camera (Chen et al., 2018) with a spatial resolution of 16 m were used. These data were downloaded from United States Geological Survey (USGS) (<http://www.usgs.gov/>) and the China Center for Resources Satellite Data and Application (<http://www.cresda.com/>), respectively. The specifications of Landsat and Gaofen-1 images were listed in Table 1. Only cloud-free images from the end of December to January of the following year were considered due to two reasons. Firstly, the dates should be synchronized to ensure the images were captured in similar hydrological and environmental conditions. Secondly, vegetation coverage in lakes is at its minimum during this time period in winter. Table 2 lists the images used for method evaluation.

To prepare satellite images for aquaculture ponds extraction, radiometric and atmospheric corrections for Landsat and Gaofen-1 images were implemented by using the radiometric calibration and

**Table 2**

Satellite images for extracting aquaculture ponds. (\*The asterisked images were used for training data selection.)

Date	Satellite	Sensor	Path/Row (longitude/latitude)	Spatial resolution (m)
2011.01.15	Landsat-5	TM	123/039	30
2014.01.23*	Landsat-8	OLI	123/039	30
2015.01.03	Landsat-8	OLI	122/039	30
2013.12.29*	Gaofen-1	WFV1	$113.9^{\circ}\text{E}, 29.6^{\circ}\text{N}$	16
2015.01.22	Gaofen-1	WFV1	$113.9^{\circ}\text{E}, 29.6^{\circ}\text{N}$	16

FLAASH atmospheric correction tool in ENVI 5.3. All images were georeferenced to the Universal Transverse Mercator (UTM) projection and coordinate system.

High-resolution satellite images from the free-accessible Google Earth platform are commonly used as ground-truth (Han et al., 2014). Unfortunately, images with dates close to the acquisition dates of the experimental images are not available from Google Earth. Therefore, 2 m-resolution digital orthophoto images derived from Level 3 production of TH-1 satellite (Zhou et al., 2015) are chosen as the reference data. The orthophoto images are acquired 19 days after the acquisition date of the 2011 Landsat TM test image, and the same day as the acquisition date of the 2015 Landsat OLI test image, and 19 days before the acquisition date of the 2015 Gaofen-1 test image. Aquaculture ponds and natural lakes can be visually identified in Liangzi Lake using these high resolution TH-1 images.

## 3. Methodology

This paper presents a SVM classification method that incorporates geometric features to separate aquaculture ponds from natural water surfaces using multi-spectral satellite images from Landsat and Gaofen-1. The water pixels were extracted using water indices and thresholding methods from multi-spectral remote sensing images. The resulted water pixels not only include natural water bodies, but also the surrounding aquaculture ponds. Following that, all water pixels are labeled into small water segments based on pixel connectivity. Once all water pixels are separated into segments, geometrical features, including area, perimeter and contour-based regularity of the water segments are calculated. Feature vectors formed by these geometrical features are then used as inputs for the SVM classifier that is trained by an established training set. The water segments are classified either as aquaculture ponds or natural water surfaces by the trained SVM classifier. Using approximately synchronous digital orthophoto (2 m resolution) as the reference data, the water body extraction and classification results are

**Table 1**  
Satellite instruments for remotely sensed imagery.

Sensor	Spatial resolution (m)	Spectral range ( $\mu\text{m}$ )	Acronym for band
Landsat TM	30	Band 1:0.450–0.520 Band 2:0.520–0.600 Band 3:0.630–0.690 Band 4:0.760–0.900 Band 5:1.550–1.750 Band 7:2.080–2.350	B G R NIR MIR SWIR
Landsat OLI	30	Band 2:0.450–0.515 Band 3:0.525–0.600 Band 4:0.630–0.680 Band 5:0.845–0.885 Band 6:1.560–1.660 Band 7:2.100–2.300	B G R NIR MIR SWIR
Gaofen-1 WFV	16	Band 1:0.450–0.520 Band 2:0.520–0.590 Band 3:0.630–0.690 Band 4:0.770–0.890	B G R NIR

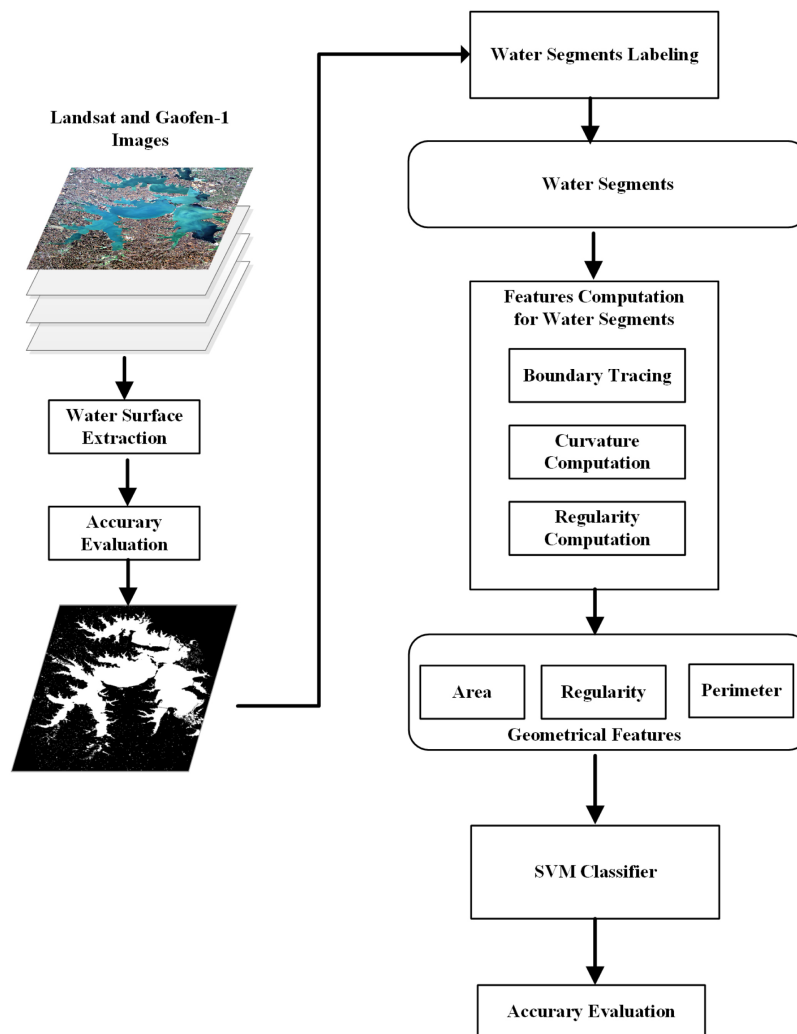


**Fig. 2.** Flowchart for the extraction and classification of aquaculture ponds and natural water surfaces.

validated by manually digitized and labeled water types. The flow chart of the proposed method is shown in Fig. 2.

### 3.1. Water surface extraction and water segments labeling

The water surface extraction is implemented by thresholding the water index images that are calculated using reflectance values in different spectral bands from multi-spectral satellite images. Water index images can be produced by MNDWI, MNDWI and NDWI (cf. Table 3). The water index that best discriminates water and non-water surfaces is chosen for each sensor, including Landsat TM, OLI and Gaofen-1 WVF.

Because a gray-scale water index image usually exhibits a bimodal histogram (water and non-water), the extraction of water pixels can be accomplished by thresholding. The threshold  $I_{threshold}$  is automatically calculated using the Ostu method (Otsu, 1979). Then the pixels with water index values less or greater than the determined  $I_{threshold}$  are separated into water or non-water. The threshold  $I_{threshold}$  is determined when the ratio of interclass variance to intra-class achieves the maximum. As shown in Fig. 3, the blue curve depicts the bimodal histogram of a water index image, while the black curve depicts the ratio between the interclass variance and the intraclass variance for each candidate threshold. The threshold with the maximum ratio (the red vertical line) is selected as the threshold for water and non-water separation using the water index image.

The water and non-water binary images generated by thresholding the water index images are partitioned into water segments using connected component labeling (Gonzalez and Woods, 2006). Each water segment is labeled as an object that will be classified into aquaculture ponds and natural water surfaces in future steps. Object based

**Table 3**  
Accuracy assessment of water extraction by various water indices.

Sensor	Index	Overall accuracy (%)	Kappa	Producer's accuracy (%)	User's accuracy(%)
OLI	NDWI	95.8	0.880	84.1	98.1
	MNDWI	<b>96.0</b>	<b>0.883</b>	83.9	98.9
	AWEI	85.4	0.631	83.0	64.9
	NDVI	95.9	0.882	<b>84.6</b>	97.9
	WRI	93.7	0.808	73.5	<b>99.8</b>
	NDMI	86.2	0.633	76.8	68.6
TM	NDWI	97.2	0.914	90.5	96.1
	MNDWI	<b>97.6</b>	<b>0.928</b>	91.6	97.1
	AWEI	84.9	0.616	88.5	59.7
	NDVI	97.2	0.917	<b>92.3</b>	94.6
	WRI	97.1	0.908	87.8	<b>98.1</b>
	NDMI	92.7	0.793	91.4	77.8
Gaofen-1	NDWI	<b>96.0</b>	<b>0.885</b>	85.8	<b>96.9</b>
	NDVI	95.7	0.877	<b>86.5</b>	94.8

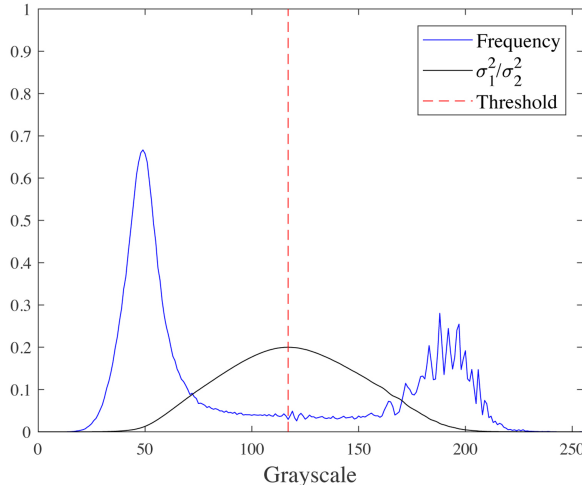


**Fig. 3.** Optimal threshold determined using OSTU method for water and non-water discrimination.  $\sigma_1^2$  denotes the interclass variance, and  $\sigma_2^2$  denotes the intraclass variance.

classification can employ support vector machine to accomplish the separation of aquaculture ponds and natural water surfaces.

### 3.2. Features computation for water segments

The extracted water segments are then considered as two categories: natural water surfaces and aquaculture ponds. To achieve the separation of these two categories, characteristics that can discriminate aquaculture ponds from natural water surfaces are explored.

#### 3.2.1. Contour-based regularity measure for water segments

Contours of naturally-formed water surfaces generally follow the local terrain. On the contrary, aquaculture ponds commonly have regular boundaries composed by straight lines that are artificially constructed to minimize the construction costs. Man-made dykes or levees are straight lines that disrupt the smooth bending surfaces of natural water surfaces as shown in remote sensing images. Therefore, contour-based regularity is proposed to depict the difference in geometry for natural water surfaces and aquaculture ponds. The contour-based regularity of a water body is defined using following formula:

$$R = \frac{s_{\kappa=0}}{s_{\text{all}}} \quad (1)$$

$s_{\kappa=0}$  is the sum of arc length with zero curvature on the boundary and  $s_{\text{all}}$  is the total arc length of the boundary. Curvature is the bending degree of a curve. As digital images are discrete representations of real world objects, the curvature for each pixel of a contour lines is calculated by approximation, using the change of angle along the curved path (Nixon and Aguado, 2012). Thus, the curvature for each pixel along the boundary of a water body can be computed using

$$\kappa(t) = \frac{d\phi(t)}{ds} \quad (2)$$

where  $s$  is arc length, the curvature gives the change of a direction  $\phi(t)$  with respect to arc length.

Contour-based regularity globally measures the percentage of straight parts in a boundary, and depicts a degree of contour-based regularity for the water body. A natural lake surface tends to fit the local terrain that its boundary pixels mostly have non-zero curvature. Thus,  $R$  values tends to be small for natural lakes. On the contrary, the boundary of an aquaculture pond is artificially constructed and straight. The boundary of aquaculture ponds mostly consist of zero-curvature points. Thus,  $R$  values tend to be large for aquaculture ponds.

#### 3.2.2. Feature vector computation for water segments

The feature vector for a water body segment is mainly geometrical features including area, perimeter and contour-based regularity. Area is computed by counting the pixels of a water segment during the connected component labeling process, while other geometrical features are calculated during boundary tracing to get the inner boundary of a water segment. The boundary tracing process is employed as a frame of implementing curvature computation at each boundary pixel for a water segment. Then, curvature can be computed along the contour of a water segment. In the end, contour-based regularity is calculated based on the curvature values for all boundary pixels.

**Boundary tracing.** Boundary tracing uses the chain code (Sonka et al., 2014),  $CC = \{0, 1, \dots, 7\}$ , which presents the eight directions of a pixel in the image (Fig. 4(a)). In the process, assuming that the current pixel identified as a border pixel is  $P_i$ , the previous one as a border pixel is  $P_{i-1}$ , and the next one as a border pixel is  $P_{i+1}$ . The direction of  $P_i$  to  $P_{i-1}$  is  $\phi_{i-1}$ , the direction of  $P_{i+1}$  to  $P_i$  is  $\phi_i$ . Thus,  $\phi_{i-1}$  and  $\phi_i$  can be presented as the chain code, i.e.  $\phi_{i-1}, \phi_i \in CC$ . The arc length between  $P_{i-1}$  and  $P_i$  is  $s_{i-1}$ , and the arc length between  $P_i$  and  $P_{i+1}$  is  $s_i$ , as shown in Fig. 4(b). The

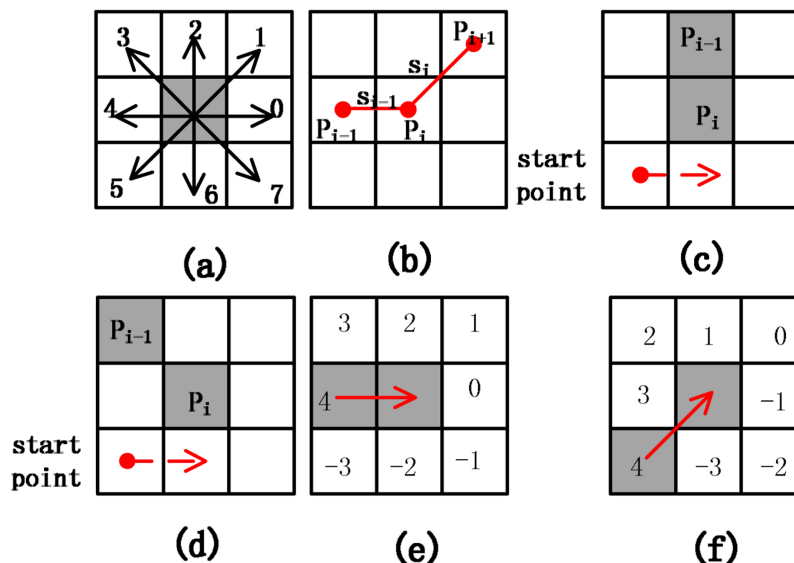


**Fig. 4.** Boundary tracing and curvature computation.

framework mainly consists of three steps (described in Algorithm 1 in detail):

- step 1** search for the first boundary pixel of a water segment from the upper left of the image and initialize it;
- step 2** boundary tracing(Sonka et al., 2014) and curvature calculation at each boundary pixel;
- step 3** contour-based regularity computation for a water segment.

#### Algorithm 1

---

##### Algorithm 1: contour-based regularity computation for a water segments

---

```

/* step 1: searching the first boundary pixel of new water segment */
1 i ← 1, sall ← 0, sκ=0 ← 0
2 Find first pixel of a water segment from top left of a image, set this pixel as Pi, and
   φi-1 ← 7
/* step 2: boundary tracing and curvature computation */
3 repeat
   /* tracing border */
   4 Get the start point in the 8-connectivity neighborhood of Pi at the direction of
   5 if φi-1 is even then (φi-1 + 7) mod 8/* Figure4(c) */ 
   6 if φi-1 is odd then (φi-1 + 6) mod 8/* Figure4(d) */
   7 In 8-connectivity neighborhood, search the first pixel with the same value as Pi in an
      anti-clockwise direction from start point and set it as Pi+1
   /* Pi+1 is a new boundary pixel */
   8 φi ← the 8 connectivity direction of Pi+1 from Pi
   /* Curvature computation */
   9 Δφ ← (φi - φi-1)
  10 if Δφ > 4 or Δφ <= -4 then Δφ ← Δφ mod 8
  11 if φi-1 is even then si-1 ← 1 else si-1 ← √2
  12 if φi is even then si ← 1 else si ← √2
  13 κ ← π/4 × Δφ / (si + si-1) / 2
  14 sall ← sall + (si + si-1) / 2
  15 if κ equals to zero then s0 ← s0 + (si + si-1) / 2
  16 i ← i + 1
  17 until the pixel Pi returns the pixel P1
/* step 3:contour-based regularity computation */
18 R ← sκ=0 / sall

```

---

**Curvature computation.** Curvature is a derivative of the turning angle with respect to arc length, as shown in Eq. (2). The curvature at pixel P<sub>i</sub> can be evaluated by the ratio between the difference of φ<sub>i</sub> and φ<sub>i-1</sub> to the arc length during boundary tracing. The direction change can be evaluated by chain code difference between φ<sub>i</sub> and φ<sub>i-1</sub>, which ranges from -3 to 4, as shown in Fig. 4(e) and (f). The arc length takes the

boundary length in the pixel P<sub>i</sub>, i.e.  $\frac{s_i + s_{i-1}}{2}$ . See lines 11–17 of Algorithm 1 in details.

**Contour-based regularity computation.** The contour-based regularity of a water body segment can be measured by the proportion of straight parts in its boundary over the entire boundary. The sum of boundary length for all pixels with a curvature of zero can be recorded during boundary tracing. When the boundary tracing procedure is completed, the contour-based regularity of a water body segment can be evaluated using Formula (1). In Algorithm 1, lines 18–19 describe how to record the total length of a water segment

boundary and the length of the partial boundary with zero curvature and line 22 computes the contour-based regularity.

#### 3.3. Aquaculture ponds and natural water surfaces classification

SVM has been extensively applied for remote sensing classification tasks as a supervised method using an optimal hyperplane to separate

the data set into different classes, especially in circumstances with limited training samples (Huang et al., 2002; Mountrakis et al., 2011; Han et al., 2014; Wang et al., 2014). SVM is used for aquaculture ponds and natural water surfaces classification in the paper. Geometrical features, such as perimeter, area and contour-based regularity, are integrated into feature vectors as input features. The C-support vector classification model is adopted for SVM classification (Cortes and Vapnik, 1995), in which the Gauss kernel function is used. The parameters of SVM classifier are optimized by the sequential minimal optimization (SMO) algorithm in the training data set (Platt, 1998).

### 3.3.1. Training datasets

Geometrical features including area, perimeter and contour-based regularity are spatial resolution dependent. Thus, different training datasets should be prepared for images with different spatial resolutions. Since TM and OLI sensors have similar spatial resolution, the training datasets for Landsat images are all from an OLI image acquired on January 23, 2014. The training data for all Gaofen-1 images is from a Gaofen-1 image acquired on December 29, 2013. From these images, aquaculture ponds and natural water reference data are selected and used to train the SVM classifier. The training data are labeled into two classes: natural water body and aquaculture pond.

### 3.3.2. Feature selection

Several geometrical features of water segments are compared in this study: area; perimeter; ratio of the squared perimeter to area (P2A); Compactness ratio C (Ottinger et al., 2017), which is the square root of the ratio of area divided by the area of a circle with the perimeter; rectangluarity (Rosin, 2003), which is the ratio between the area of the water body and its minimum bounding rectangle; structural line-based regularity (Wang et al., 2017), which describes highly structural (parallel or perpendicular) line segments of a regions, and contour-based regularity, which describes the percentages of straightness in the boundary of water body. Among them, compactness, rectangluarity, structural line-based regularity and contour-based regularity are the four features that geometrically describe a water body from different perspectives. To find the best feature combination for the discrimination of aquaculture ponds and natural water surfaces, the feature combination of perimeter, area and contour-based regularity (PACReg) is compared with the other feature combinations: (1) two basic feature which are area and perimeter (PA); (2) perimeter, area, P2A, and Compactness (PACompC); (3) perimeter, area and rectangluarity (PARec); (4) perimeter, area and structural line-based regularity (PALReg). The PACReg is selected as the feature combination for its comprehensively best performance (see Section 4.2).

### 3.3.3. Feature normalization

In the training stage, all features should be normalized to ensure these values are scaled to the same range for the SVM classifier. Feature normalization uses a linear model that scale the values to the same range, for example, the  $j$ th feature  $x_j^{(i)}$  of the  $i$ th training sample, which needs to be normalized into the range of  $[l, u]$ , the formula is as follows:

$$x_{ij}^{\text{norm}} = l + (u - l) \frac{x_j^{(i)} - \min x_j}{\max x_j - \min x_j} \quad (3)$$

**Table 4**  
Accuracy assessment for water surface extraction using multispectral images.

Study area	Image sensors	Overall accuracy (%)	Kappa	Producer's accuracy (%)	User's accuracy (%)
Eastern Liangzi Lake	TM	86.3	0.726	79.8	91.8
Eastern Liangzi Lake	OLI	89.2	0.784	78.5	97.8
Eastern Liangzi Lake	Gaofen-1	88.8	0.764	76.6	95.8
Western Liangzi Lake	TM	97.1	0.915	89.7	97.3
Western Liangzi Lake	OLI	96.5	0.898	85.8	99.2
Western Liangzi Lake	Gaofen-1	96.1	0.884	85.0	97.5

$x_j$  is  $j$ th attribute values from all objects.

### 3.4. Validation

The reference data for water bodies are drawn manually from the digital orthoimage (2 m resolution) of the two experimental areas. All water pixels are labeled as natural water surface and aquaculture pond by visual interpretation and further confirmed by field investigation. Both the results of water pixel extraction and water surfaces classification are validated using the reference data. First, 2000 pixels are randomly generated in the study regions from the water extraction results. The water or non-water labels are compared with the reference data. The results from SVM classification are also verified by 2000 pixels randomly generated. The labels of water categories from the reference data are used to discriminate whether a random pixel has been successfully classified as aquaculture ponds or natural water.

## 4. Results

### 4.1. Water surface extraction results

By comparing the accuracy of water surface extraction of various water indices applied to the experimental images (Rokni et al., 2014; Feyisa et al., 2014), including NDWI, MNDWI, NDMI, WRI, AWEI and NDVI (Normalized Difference Vegetation Index, Rokni et al., 2014), the best water index compatible with each sensor is decided for Landsat TM, OLI and Gaofen-1 WVF. The water index with the highest overall accuracy in water extraction is chosen. As indicated in Table 3, MNDWI achieves the best water/non-water separation for Landsat TM and OLI, while NDWI works best for Gaofen-1 WVF.

Table 4 presents the accuracy of water Surface extraction in the two experimental regions using different satellite sensors. The Overall Accuracy (OA) of water extraction is at least 96% for western Liangzi Lake and at least 86.3% for eastern Liangzi Lake. The User's Accuracy (UA) can score up to 99.2% in western Liangzi Lake and 97.8% in eastern Liangzi Lake. The Producer's Accuracy (PA) can reach 89.7% in western Liangzi Lake and 79.8% eastern Liangzi Lake. The accuracies of surface water extraction from different sensors are similar for the same region. However, the accuracies vary greatly for different regions, with higher accuracy in the western region than in the eastern region. Because small-sized ponds are more densely distributed in eastern study region than in the western region, leading to many pixels partially covered by water and land on medium spatial resolution images. As the reference data have a 2 m resolution, while the images used for water extraction have much lower spatial resolution (30 m for Landsat TM and OLI and 16 m for Gaofen-1), several small water bodies that can be identified from the digital orthophotos might disappear in Landsat or Gaofen-1 images. Fig. 5 demonstrates the results of surface water pixel extraction in eastern Liangzi Lake from Landsat TM, OLI and Gaofen images.

### 4.2. Natural water surfaces and aquaculture ponds classification

Table 5 lists the accuracy of water surface classification using geometrical features that include area, perimeter and contour-based regularity. The OA all exceed 94% with kappa coefficients above 0.8. The

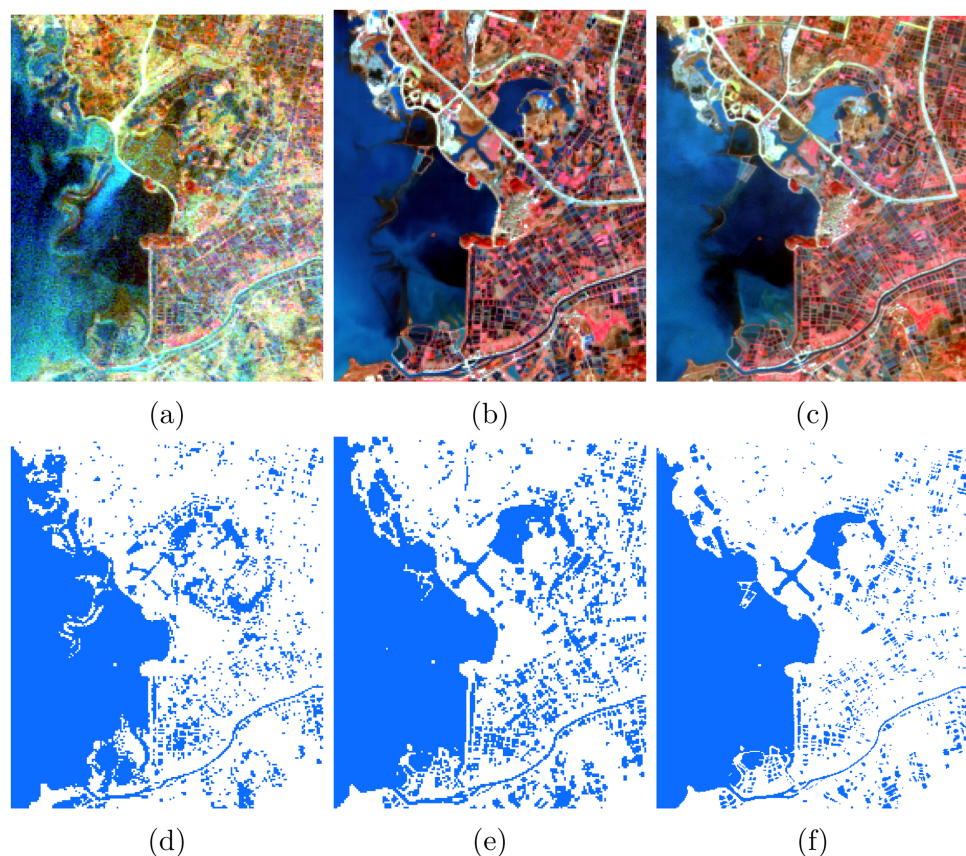


**Fig. 5.** Results of surface water extraction. (a)–(c) are respectively TM, OLI and Gaofen-1 images of eastern Liangzi Lake region, which were captured on January 15, 2011, January 3, 2015 and January 22, 2015, respectively. (d)–(f) are surface water extraction results of (a)–(c).

PA and UA for natural water all exceed 96%, while the corresponding values for aquaculture pond can also reach more than 90%. No significant difference in classification accuracy for the two study regions, proved that the proposed feature combination and classifier had stable performance in different study areas. As shown in Fig. 6, the proposed method can clearly classify water bodies into natural water surfaces and aquaculture ponds using images from three different sensors.

The OA and Kappa coefficients for PACReg are almost always better than other feature combinations (Table 6), meaning that PACReg has the best overall performance. However, when PA and UA for aquaculture ponds and nature water surfaces are examined, PACReg are not always the best. Fig. 7 demonstrates the classification results of different feature combinations in Gaofen-1 image of eastern Liangzi Lake. When PA is used, the classifier separates aquaculture ponds from natural water surfaces simply by dividing water segments in size. For instance, the cross shaped water surface and the one on its right are misclassified into aquaculture pond in Fig. 7(a). PACCompC uses P2A and Compactness C, which works well for coastal delta region (Ottinger et al., 2017). For the aquaculture ponds around inland lake area in this

study, the overall accuracy of PACCompC is not as good as the proposed feature combination (PACReg). For instance, a river is not recognized and erroneously classified into aquaculture pond as shown in Fig. 7(b), because compactness is incapable of describing the shape dissimilarity between a natural water surface and an aquaculture pond. When the producer's and user's accuracy were considered, PARec is superior in only a few cases that aquaculture ponds are separated correctly. Because rectangularity can well depict water segments with almost rectangular shape, but can not depict the curvature of nature water surfaces that have many small twists and turns. For example, the big lake and the river are wrongly classified as aquaculture ponds in Fig. 7(c). Even though structural line-base regularity succeed in identifying raft cultivation area as in Wang et al. (2017), which evaluates the percentage of parallel or perpendicular lines in relation to a region, PALReg misclassify the cross shaped water surface and the one on its right as ponds which were actually natural waters (fig:ResultclassFig. 7(d)). This suggests that the structural line-base regularity is not suit to distinguish the aquaculture ponds from the natural water bodies in neighboring area of inland lake. Fig. 7(e) is the result using PACReg.

**Table 5**

Accuracy assessment for aquaculture ponds and natural water surfaces classification (A: Eastern Liangzi Lake; B: Western Liangzi Lake).

Study area	Sensors	Overall accuracy (%)	Kappa	Producer's accuracy		User's accuracy	
				Natural water (%)	Aqua-culture (%)	Natural water (%)	Aqua-culture(%)
A	TM	94.5	0.860	96.2	90.0	96.3	90.0
A	OLI	96.8	0.892	98.7	88.3	97.4	94.1
A	Gaofen-1	98.1	0.924	99.5	90.0	98.2	97.2
B	TM	97.4	0.806	98.3	85.5	98.9	78.7
B	OLI	96.9	0.856	97.2	94.7	99.3	81.1
B	Gaofen-1	97.3	0.841	98.7	83.7	98.3	87.5

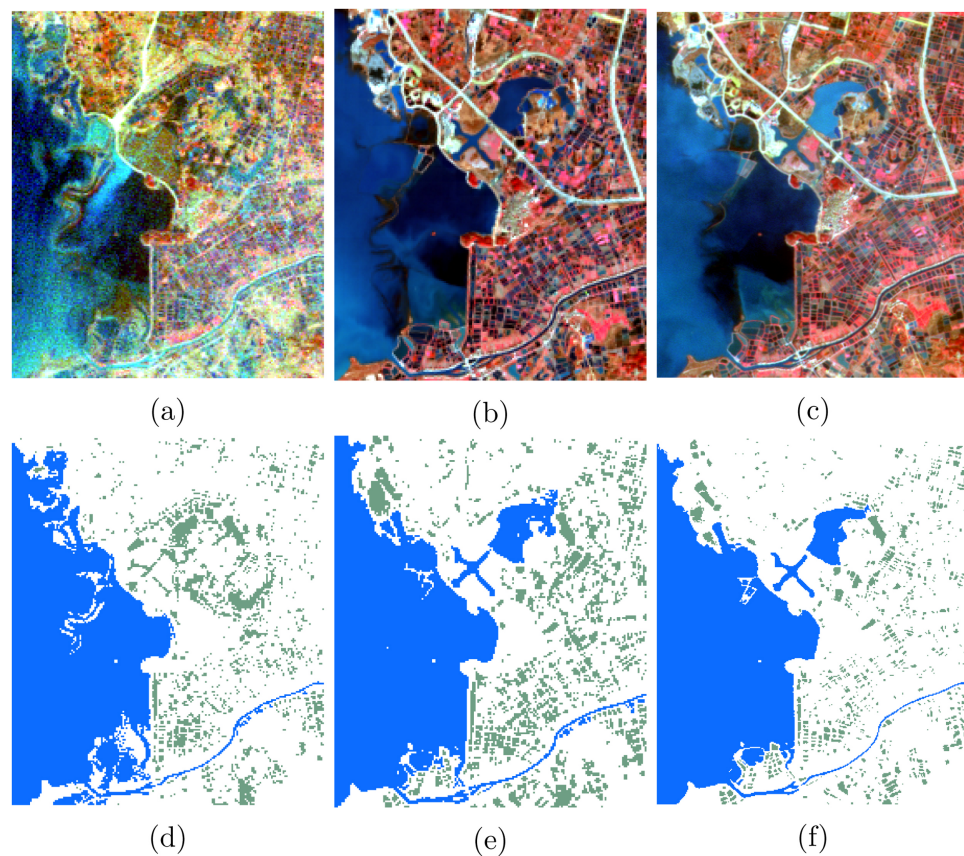


**Fig. 6.** Classification results of the SVM classifier using area, perimeter and contour-based regularity as the geometric features. Areas in blue stand for natural water surfaces and areas in cyan represent aquaculture ponds. (a)–(c) are images of eastern Liangzi Lake from TM, OLI and Gaofen-1, respectively. (d)–(f) are the corresponding classification results of (a)–(c). The cross-shaped water surface with the lake on its right as shown in (e) and (f) were reclaimed natural water surfaces from aquaculture ponds after 2013, thus these locations are covered by aquaculture ponds in (d) when (a) was acquired in 2011. (For interpretation of the references to color in this figure legend, the reader is referred to the web version of this article.)

**Table 6**  
Classification accuracies for different combinations of features in Eastern and western lake for TM, OLI and GeoFen-1.

Study area	Sensor	Feature combination	Overall accuracy (%)	Kappa	Producer's accuracy		User's accuracy	
					Natural water (%)	Aqua-culture (%)	Natural water (%)	Aqua-culture (%)
Eastern	OLI	PA	92.2	0.763	92.6	<b>90.6</b>	97.8	73.4
		PACompC	96.1	0.872	97.5	90.1	97.8	89.0
		PARec	92.2	0.763	92.6	<b>90.6</b>	97.8	73.5
		PALReg	92.3	0.753	92.6	<b>90.6</b>	<b>98.0</b>	71.5
		<b>PACReg</b>	<b>96.8</b>	<b>0.892</b>	<b>98.7</b>	88.3	97.4	<b>94.1</b>
	TM	PA	94.2	0.851	95.6	<b>90.1</b>	<b>96.4</b>	88.2
		PACompC	93.5	0.830	<b>96.4</b>	85.4	94.8	<b>89.6</b>
		PARec	94.2	0.851	95.7	<b>90.1</b>	<b>96.4</b>	88.2
		PALReg	92.9	0.821	94.4	88.8	95.8	85.3
		<b>PACReg</b>	<b>94.5</b>	<b>0.860</b>	96.2	89.9	96.3	89.5
	GaoFen-1	PA	92.8	0.745	93.2	90.3	98.2	69.8
		PACompC	97.3	0.893	98.6	89.9	98.2	91.8
		PARec	20.2	0.019	6.4	<b>99.6</b>	<b>98.9</b>	15.7
		PALReg	90.6	0.667	90.8	88.9	98.1	60.8
		<b>PACReg</b>	<b>98.1</b>	<b>0.924</b>	<b>99.6</b>	89.9	98.3	<b>97.3</b>
Western	OLI	PA	93.5	0.739	92.8	<b>99.1</b>	<b>99.9</b>	63.6
		PACompC	<b>97.1</b>	0.853	<b>98.7</b>	85.0	98.1	<b>88.9</b>
		PARec	93.5	0.739	92.8	<b>99.1</b>	<b>99.9</b>	63.6
		PALReg	92.4	0.695	91.6	<b>99.1</b>	<b>99.9</b>	58.5
		<b>PACReg</b>	96.9	<b>0.856</b>	97.2	94.7	99.3	81.1
	TM	PA	91.7	0.567	91.5	<b>94.2</b>	<b>99.5</b>	44.9
		PACompC	97.3	0.780	<b>99.0</b>	75.4	98.2	<b>83.9</b>
		PARec	91.7	0.567	91.5	<b>94.2</b>	<b>99.5</b>	44.9
		PALReg	90.4	0.498	90.3	93.3	<b>99.5</b>	38.1
		<b>PACReg</b>	<b>97.4</b>	<b>0.806</b>	98.3	85.5	98.9	78.7
	GaoFen-1	PA	<b>97.7</b>	<b>0.872</b>	98.4	<b>91.3</b>	<b>99.1</b>	85.7
		PACompC	96.3	0.758	<b>99.2</b>	68.5	96.8	<b>90.0</b>
		PARec	10.5	0.013	1.9	<b>91.3</b>	68.0	8.9
		PALReg	96.7	0.823	97.7	86.9	98.5	81.6
		<b>PACReg</b>	97.3	0.841	98.7	83.7	98.3	87.5



**Fig. 7.** Classification results using different feature combinations for Gaofen-1 image of eastern Liangzi Lake. (a)–(e) are classification results using PA, PACompC, PARec, PALReg and PACReg, respectively. The areas in blue stand for natural lakes and the areas in cyan represent aquaculture ponds. (For interpretation of the references to color in this figure legend, the reader is referred to the web version of this article.)

Contour-based regularity portrays the difference in shape between man-made aquaculture ponds and natural water surfaces, and can correctly identify the river and the cross shaped water surface. The above results demonstrate that contour-based regularity is most effective in differentiating aquaculture ponds from natural water surfaces, because contour-based regularity feature essentially depicts the shape difference between these two types.

The boundaries of aquaculture ponds are more regular than those of natural water segments as shown in Fig. 8. The contour-based regularity plays a key role in correctly classifying aquaculture ponds from natural water surfaces in the two study regions. In western Liangzi Lake region, the neighboring areas have been transformed into aquaculture ponds partially, resulting in a mixture of natural water bodies and aquaculture ponds as shown in Fig. 9. The classification of these areas using the proposed method is predominantly correct when compared with the results of visual interpretation and field investigation. As shown in Fig. 9(b) and (e), the classifier that combines contour-based regularity with perimeter and area identifies the two water segments with irregular shape and curved boundary as natural water surfaces, which is confirmed by field investigation. In Fig. 9(c) and (d), the areas neighboring lake shores are reconstructed into aquaculture ponds. The proposed method works properly to separate aquaculture pond and natural

water surfaces as demonstrated in Fig. 9(f) and (g).

As shown in Fig. 1, a stretch of aquaculture ponds that resemble a regular lattice are located in eastern Liangzi Lake. As demonstrated in Fig. 10(e)–(g), the contour-based regularity feature can correctly identify aquaculture ponds and natural water surfaces not only in Gaofen-1 image with 16 m resolution, but also in Landsat TM and OLI images with 30 m resolution. Especially, a river in the lower part is correctly recognized as natural water surfaces due to the curving contour. However, due to the relatively low spatial resolution of Landsat, some aquaculture ponds can hardly be distinguished from each other or from natural water surfaces. Thus, ponds that were small in size and close to each other were merged in the water extraction stage. Nonetheless, most of the borders after merging are still straight, the contour-based regularity feature still plays a role in the classification of aquaculture ponds and natural water surfaces. However, a few pixels close to the ponds become a mixture of water and other objects in the Landsat classification results when compared to that of Gaofen-1 image. For example, in Fig. 6(d) and (e), a few aquaculture ponds that were close to the river were misclassified as natural water bodies because they were identified as connected to the river in the surface water extraction stage.



**Fig. 8.** Field photos taken for the study area. The Landsat OLI images on the top-left and top-center showed the locations where field photos were taken for western and eastern Liangzi lake, respectively. (A) A natural lake recovered after 2013 with irregular boundaries. (B) A typical aquaculture pond with regular borders. Two pumps can be seen on its left bank. (C) A branch of Liangzi Lake with irregular border. (D) A natural water surface with irregular boundaries that follow the local terrain. (E) An aquaculture pond transformed from a neighboring area of Liangzi Lake with an aquarium air pump equipped in the center.

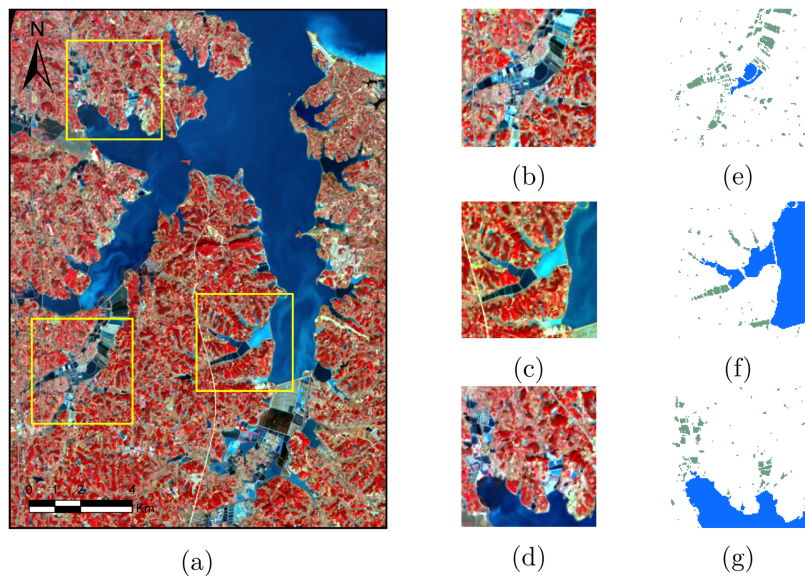


**Fig. 9.** Classification results in three typical areas of western Liangzi Lake. (a) OLI image of western Liangzi Lake with three typical areas marked in yellow rectangles. (b)–(d) are magnified display for the three typical areas. (e)–(g) are the corresponding classification results of (b)–(d). (For interpretation of the references to color in this figure legend, the reader is referred to the web version of this article.)

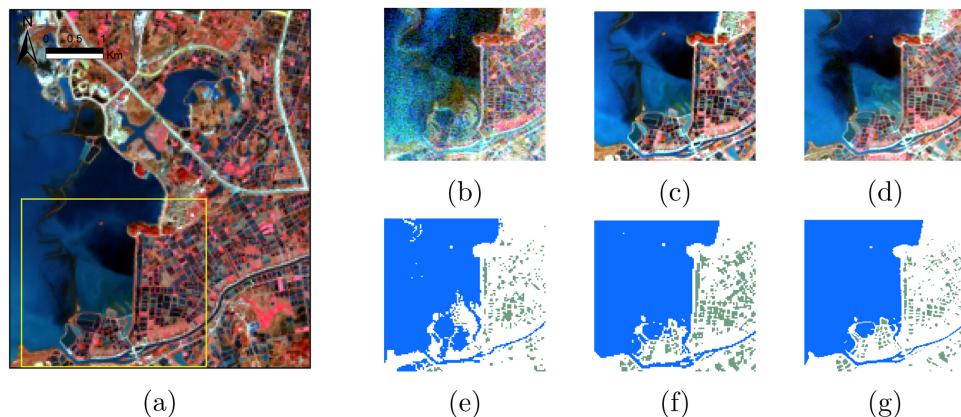


**Fig. 10.** Classification results for a typical area of eastern Liangzi Lake. (a) OLI image of eastern Liangzi Lake with a typical area shown in a yellow box. (b)–(d) are magnified display for the typical area from TM, OLI and Gaofen-1 images, respectively. (e)–(g) are the corresponding classification results of (b)–(d). (For interpretation of the references to color in this figure legend, the reader is referred to the web version of this article.)

## 5. Discussion

The shore area of Liangzi Lake have been gradually transformed into aquaculture ponds due to human interference, resulting in many small aquaculture ponds scattered around the lake. The mixing of aquaculture ponds with natural water surfaces poses great challenges for the extraction of aquaculture ponds using commonly defined features. The proposed method with contour-based regularity can correctly extract aquaculture ponds in most cases. However, the proposed method incorrectly distinguished a few aquaculture ponds and natural water bodies. The coarse spatial resolution of the satellite images compared to the small size of ponds was the main reason. As human made embankments were built in the water surfaces near the shore, natural water bodies were transformed into aquaculture ponds. However, the width of embankments are small compared to the coarse spatial resolution of medium-resolution satellite images, leading to the mixing of water spectrum and embankment spectrum. Thus, the embankment pixels were incorrectly classified as natural water bodies. Take the circled region A in Fig. 11 as an example, the straight embankment that split aquaculture ponds, which was a line segment geometrically, was wrongly classified as water surfaces in the water extraction stage, resulting in the lack of embankment after water body extraction. However, these man-made straight embankments are the most important features to distinguish ponds and natural surfaces. The missing of these straight embankments would weaken the regular features in the boundary, leading to the misclassification of ponds.

The lack of true synchronization between experimental and high-

resolution reference images poses another problem for accuracy assessment. Because in winter during the dry season for Liangzi Lake, water is frequently transferred from one aquaculture pond to another either for harvesting or water transferring. Thus, the date difference between the classification image and the reference image can lead to some discrepancies, which may also influence the classification accuracy slightly.

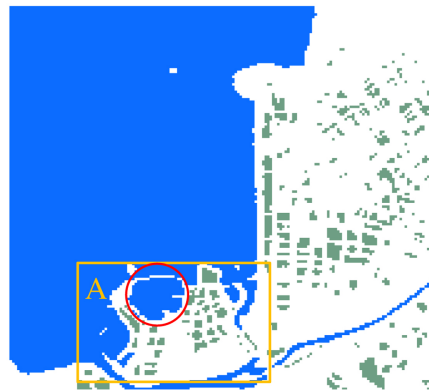
SVM is chosen as the classification model because it is a prevailing machine learning method with good generalization that employs limited trained samples (Mountrakis et al., 2011; Heydari and Mountrakis, 2018). Because high-resolution images that were synchronized with the medium-resolution multi-spectral images are rare, the reference data for training is limited in this study. Thus, the generalization performance of SVM can better meet this limitation. Moreover, the dimensions of feature space are not high. The points representing natural water bodies and aquaculture ponds can cluster respectively in the feature space incorporating the dimension of contour-based regularity, meaning that SVM can easily construct a hyperplane dividing the data into two classes. SVM is less computationally intensive than other classification models. Random forest (RF) may be an alternative model for water segments classification because it is another popular machine learning method with good performance in remote sensing community (Li et al., 2016). Fig. 12 compares the classification results for these two commonly used models in the context of this study. It can be seen that the classification accuracies of SVM are comprehensively better compared to that of random forest, even though the RF is slightly better for OLI images.



(a)



(b)



(c)

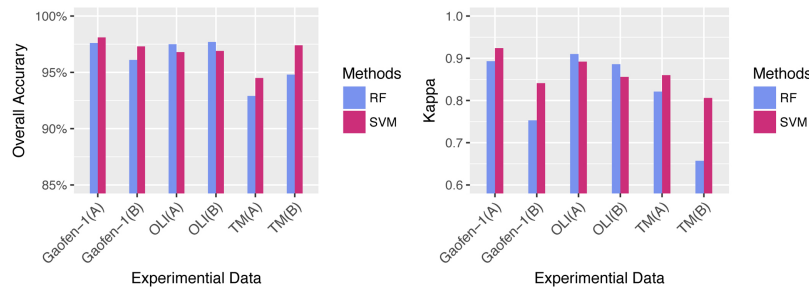


**Fig. 12.** The classification results of random forest and SVM, using area, perimeter and proposed contour-based regularity. X axis labels stand for experimental images, where A and B respectively represent eastern and western Liangzi Lake.

## 6. Conclusions

This paper presents an approach of exploiting Support Vector Machine (SVM) classification based on geometrical features that include perimeter, area and contour-based regularity for the separation of aquaculture ponds nearby inland lake regions. A contour-based regularity feature was proposed to facilitate the extraction of aquaculture ponds from Landsat TM and OLI images as well as Gaofen-1 WVF images. This regularity feature operates based on the premise that the contours of aquaculture ponds are more regular than that of natural lakes from medium resolution satellite images. Using the proposed feature, a method for aquaculture ponds extraction from the area of inland lakes is presented for multi-spectral satellite images with spatial resolution of 16–30 m (less than 10 m). The experiment results indicate that the proposed method can effectively separate aquaculture ponds from natural water bodies in Landsat TM and OLI as well as in Gaofen-1 images. The SVM classification with feature combination of contour-based regularity, perimeter and area comprehensively outperform other

feature combinations for the extraction of aquaculture ponds from water bodies nearby inland lakes.

This technique, which is based on the contour-based regularity feature to identify aquaculture ponds around inland lakes in remotely sensed images, can be widely applied for lake waters monitoring. Application of such mapping techniques over all historic Landsat archive holds great potential for the continuous monitoring of the historic changes in inland lake environment. Meanwhile, Gaofen-1 images can also be used to shorten the revisit cycle to facilitate the near-real-time monitoring inland lakes in recent years. Furthermore, the proposed contour-based regularity feature can not only be useful for the extraction of artificial water ponds, but can also be used for the mapping of other regularly-shaped objects, such as buildings and many others. Future research would focus on the unmixing of pixels, as they are the main source of error in medium spatial resolution satellite images for distinguishing aquaculture ponds within areas densely distributed with ponds.

## Acknowledgements

This work was supported partially by the National Key Research and Development Program of China under Grant 2017YFC1405600, partially by the Fundamental Research Funds for the Central Universities under Grant 18CX02060A and CCNU19QN049, and partially by the National Natural Science Foundation of China under grant 41506208.

## References

- Alian, S., Tolpekin, V.A., Bijker, W., Kumar, L., 2014. Identifying curvature of overpass mountain roads in Iran from high spatial resolution remote sensing data. *Int. J. Appl. Earth Obs. Geoinf.* 26, 21–25. <https://doi.org/10.1016/j.jag.2013.05.002>.
- Bengil, F., Bizsel, K.C., 2014. Assessing the impact of aquaculture farms using remote sensing: an empirical neural network algorithm for Ildiri Bay, Turkey. *Aquacult. Environ. Interact.* 6, 67–79. <https://doi.org/10.3354/aei00115>.
- Chen, S., Liu, J., Huang, W., Chen, R., 2018. Wide swath stereo mapping from Gaofen-1 wide-field-view (WFV) images using calibration. *Sensors* 18, 739. <https://doi.org/10.3390/s18030739>. <http://www.mdpi.com/1424-8220/18/3/739>.
- Cortes, C., Vapnik, V., 1995. Support-vector networks. *Mach. Learn.* 20, 273–297. <https://doi.org/10.1007/BF00994018>.
- Eskandari, A.R., Kouchaki, Z., Definition, R.S., Sensing, R., 2012. Regular shapes detection in satellite images. *Malays. J. Comput. Sci.* 25, 56–66.
- Feyisa, G.L., Meilby, H., Fensholt, R., Proud, S.R., 2014. Automated water extraction index: a new technique for surface water mapping using Landsat imagery. *Remote Sens. Environ.* 140, 23–35. <https://doi.org/10.1016/j.rse.2013.08.029>.
- Froehlich, H.E., Gentry, R.R., Rust, M.B., Grimm, D., Halpern, B.S., 2017. Public perceptions of aquaculture: evaluating spatiotemporal patterns of sentiment around the world. *PLoS ONE* 12, 1–18. <https://doi.org/10.1371/journal.pone.0169281>.
- Gonario, S., Virdis, P., 2014. An object-based image analysis approach for aquaculture ponds precise mapping and monitoring: a case study of Tam Giang-Cau Hai Lagoon, Vietnam. *Environ. Monit. Assess.* 186, 117–133. <https://doi.org/10.1007/s10661-013-3360-7>.
- Gonzalez, R.C., Woods, R.E., 2006. *Digital Image Processing*, 3rd ed. Prentice-Hall, Inc, Upper Saddle River, NJ, USA.
- Gusmawati, N., Soulard, B., Selmaoui-Folcher, N., Proisy, C., Mustafa, A., Le Gendre, R., Laugier, T., Lemmonnier, H., 2018. Surveying shrimp aquaculture pond activity using multitemporal VHSR satellite images – case study from the Perancak estuary, Bali, Indonesia. *Mar. Pollut. Bull.* 131, 49–60. <https://doi.org/10.1016/j.marpolbul.2017.03.059>.
- Han, X., Chen, X., Feng, L., 2014. Four decades of winter wetland changes in Poyang Lake based on Landsat observations between 1973 and 2013. *Remote Sens. Environ.* 156, 426–437. <https://doi.org/10.1016/j.rse.2014.10.003>.
- Heydari, S.S., Mountrakis, G., 2018. Effect of classifier selection, reference sample size, reference class distribution and scene heterogeneity in per-pixel classification accuracy using 26 Landsat sites. *Remote Sens. Environ.* 204, 648–658. <https://doi.org/10.1016/j.rse.2017.09.035>.
- Huang, C., Davis, L.S., Townsend, J.R.G., 2002. An assessment of support vector machines for land cover classification. *Int. J. Remote Sens.* 23, 725–749. <https://doi.org/10.1080/01431160110040323>.
- Kurnianggoro, L., Jo, K.H., 2018. A survey of 2D shape representation: methods, evaluations, and future research directions. *Neurocomputing* 300, 1–16. <https://doi.org/10.1016/j.neucom.2018.02.093>.
- Li, M., Ma, L., Blaschke, T., Cheng, L., Tiede, D., 2016. A systematic comparison of different object-based classification techniques using high spatial resolution imagery in agricultural environments. *Int. J. Appl. Earth Obs. Geoinf.* 49, 87–98. <https://doi.org/10.1016/j.jag.2016.01.011>.
- McFeeters, S.K., 1996. The use of the Normalized Difference Water Index (NDWI) in the delineation of open water features. *Int. J. Remote Sens.* <https://doi.org/10.1080/014311608948714>. arXiv:bhmic00033.
- Mountrakis, G., Im, J., Ogole, C., 2011. Support vector machines in remote sensing: a review. *ISPRS J. Photogramm. Remote Sens.* 66, 247–259. <https://doi.org/10.1016/j.isprsjprs.2010.11.001>.
- Nixon, M., Aguado, A., 2012. *Feature Extraction & Image Processing for Computer Vision*, 3rd ed. Academic Press <https://doi.org/10.1016/B978-0-12-396549-3.00003-3>.
- Otsu, N., 1979. A threshold selection method from gray-level histograms. *IEEE Trans. Syst. Man Cybern.* 9, 62–66. <https://doi.org/10.1109/TSMC.1979.4310076>.
- Ottinger, M., Clauss, K., Kuenzer, C., 2016. Aquaculture: relevance, distribution, impacts and spatial assessments – a review. *Ocean Coast. Manage.* 119, 244–266. <https://doi.org/10.1016/j.ocecoaman.2015.10.015>.
- Ottinger, M., Clauss, K., Kuenzer, C., 2017. Large-scale assessment of coastal aquaculture ponds with Sentinel-1 time series data. *Remote Sens.* 9. <https://doi.org/10.3390/rs9050440>.
- Palmer, S.C., Kutser, T., Hunter, P.D., 2015. Remote sensing of inland waters: challenges, progress and future directions. *Remote Sens. Environ.* 157. <https://doi.org/10.1016/j.rse.2014.09.021>.
- Pekel, J.F., Cottam, A., Gorelick, N., Belward, A.S., 2016. High-resolution mapping of global surface water and its long-term changes. *Nature* 540, 418–422. <https://doi.org/10.1038/nature20584>.
- Platt, J., 1998. Sequential Minimal Optimization: A Fast Algorithm for Training Support Vector Machines, Technical Report.
- Qin, Y., Li, Y., Wu, L., Chen, H., Li, Z., Huang, Y., 2016. Analysis on the spatial-temporal patterns of water quality in Lake Liangzi (in Chinese). *J. Lake Sci.* 28, 994–1003.
- Rautiainen, M., Möttö, M., Stenberg, P., Ervasti, S., 2008. Crown envelope shape measurements and models. *Silva Fenn.* 42, 19–33.
- Rokni, K., Ahmad, A., Selamat, A., Hazini, S., 2014. Water feature extraction and change detection using multitemporal landsat imagery. *Remote Sens.* 6, 4173–4189. <https://doi.org/10.3390/rs6054173>.
- Rosin, P.L., 2003. Measuring shape: ellipticity, rectangularity, and triangularity. *Mach. Vis. Appl.* 14, 172–184. <https://doi.org/10.1007/s00138-002-0118-6>.
- Sheng, Y., Song, C., Wang, J., Lyons, E.A., Knox, B.R., Cox, J.S., Gao, F., 2016. Representative lake water extent mapping at continental scales using multi-temporal Landsat-8 imagery. *Remote Sens. Environ.* 185, 129–141. <https://doi.org/10.1016/j.rse.2015.12.041>.
- Shi, Y., Feng, L., Gong, J., 2017. Four decades of the morphological dynamics of the lakes in the Jianghan Plain using Landsat observations. *Water Environ. J.* 31, 353–359. <https://doi.org/10.1111/wej.12250>.
- Sonka, M., Hlavac, V., Boyle, R., 2014. *Image Processing, Analysis, and Machine Vision*. Cengage Learning.
- Sun, Q., Zhang, P., Sun, D., Liu, A., Dai, J., 2018. Desert vegetation-habitat complexes mapping using Gaofen-1 WFV (wide field of view) time series images in Minqin County, China. *Int. J. Appl. Earth Obs. Geoinf.* 73, 522–534. <https://doi.org/10.1016/j.jag.2018.07.021>.
- Tebbs, E., Remedios, J., Avery, S., Rowland, C., Harper, D., 2015. Regional assessment of lake ecological states using landsat: a classification scheme for alkaline-saline, flamingo lakes in the East African rift valley. *Int. J. Appl. Earth Obs. Geoinf.* 40, 100–108. <https://doi.org/10.1016/j.jag.2015.03.010>. <http://www.sciencedirect.com/science/article/pii/S0303243415000641>.
- Tran, H., Tran, T., Kervyn, M., 2015. Dynamics of land cover/land use changes in the Mekong Delta, 1973–2011: a remote sensing analysis of the Tran Van Thoi District, Ca Mau Province, Vietnam. *Remote Sens.* 7, 2899–2925. <https://doi.org/10.3390/rs70302899>.
- Urbanski, J.A., Wochna, A., Bubak, I., Grzybowski, W., Lukawska-Matuszewska, K., Lacka, M., Sliwinska, S., Wojtasiewicz, B., Zajaczkowski, M., 2016. Application of landsat 8 imagery to regional-scale assessment of lake water quality. *Int. J. Appl. Earth Obs. Geoinf.* 51, 28–36. <https://doi.org/10.1016/j.jag.2016.04.004>. <http://www.sciencedirect.com/science/article/pii/S0303243416300630>.
- Verpoorter, C., Kutser, T., Seekell, D.A., Tranvik, L.J., 2014. A global inventory of lakes based on high-resolution satellite imagery. *Geophys. Res. Lett.* 41, 6396–6402. <https://doi.org/10.1002/2014GL060641>. arXiv:1011.1669v3.
- Wang, J., Sheng, Y., Tong, T.S.D., 2014. Monitoring decadal lake dynamics across the Yangtze Basin downstream of Three Gorges Dam. *Remote Sens. Environ.* 152, 251–269. <https://doi.org/10.1016/j.rse.2014.06.004>.
- Wang, M., Cui, Q., Wang, J., Ming, D., Lv, G., 2017. Raft cultivation area extraction from high resolution remote sensing imagery by fusing multi-scale region-line primitive association features. *ISPRS J. Photogramm. Remote Sens.* 123, 104–113. <https://doi.org/10.1016/j.isprsjprs.2016.10.008>.
- Wu, H., Zeng, G., Liang, J., Chen, J., Xu, J., Dai, J., Sang, L., Li, X., Ye, S., 2017. Responses of landscape pattern of China's two largest freshwater lakes to early dry season after the impoundment of Three-Gorges Dam. *Int. J. Appl. Earth Obs. Geoinf.* 56, 36–43. <https://doi.org/10.1016/j.jag.2016.11.006>. <http://www.sciencedirect.com/science/article/pii/S030324341630191X>.
- Wulder, M.A., Masek, J.G., Cohen, W.B., Loveland, T.R., Woodcock, C.E., 2012. Opening the archive: how free data has enabled the science and monitoring promise of Landsat. *Remote Sens. Environ.* 122, 2–10. <https://doi.org/10.1016/j.rse.2012.01.010>.
- Wulder, M.A., White, J.C., Loveland, T.R., Woodcock, C.E., Belward, A.S., Cohen, W.B., Fosnight, E.A., Shaw, J., Masek, J.G., Roy, D.P., 2016. The global Landsat archive: status, consolidation, and direction. *Remote Sens. Environ.* 185, 271–283. <https://doi.org/10.1016/j.rse.2015.11.032>.
- Xu, H., 2006. Modification of normalised difference water index (NDWI) to enhance open water features in remotely sensed imagery. *Int. J. Remote Sens.* 27, 3025–3033. <https://doi.org/10.1080/01431160600589179>.
- Yang, F., Xu, Q., Li, B., 2017. Ship detection from optical satellite images based on saliency segmentation and structure-LBP feature. *IEEE Geosci. Remote Sens. Lett.* 14, 602–606. <https://doi.org/10.1109/LGRS.2017.2664118>.
- Zhang, D., Lu, G., 2004. Review of shape representation and description techniques. *Pattern Recognit.* 37, 1–19. <https://doi.org/10.1016/j.patcog.2003.07.008>.
- Zhang, T., Li, Q., Yang, X., Zhou, C., Su, F., 2010. Automatic mapping aquaculture in coastal zone from TM imagery with OBIA approach. In: 2010 18th International Conference on Geoinformatics. Geoinformatics 2010. <https://doi.org/10.1109/GEOINFORMATICS.2010.5567961>.
- Zhou, X., Wang, H., Huang, X., 2015. 1B level data products and application of TH-01 satellite (in Chinese). *Mod. Survey. Mapp.* 38, 3–7.
- Zhou, Y., Dong, J., Xiao, X., Xiao, T., Yang, Z., Zhao, G., Zou, Z., Qin, Y., 2017. Open surface water mapping algorithms: a comparison of water-related spectral indices and sensors. *Water (Switzerland)* 9. <https://doi.org/10.3390/w9040256>.